

# Blue-yellow emissive $\text{LaAlO}_3:\text{Dy}^{3+}$ phosphor for high bright white light-emitting diodes

Ha Thanh Tung<sup>1</sup>, Huu Phuc Dang<sup>2</sup>

<sup>1</sup>Faculty of Basic Sciences, Vinh Long University of Technology Education, Vinh Long, Vietnam

<sup>2</sup>Faculty of Fundamental Science, Industrial University of Ho Chi Minh City, Ho Chi Minh City, Vietnam

## Article Info

### Article history:

Received Oct 6, 2022

Revised Nov 2, 2022

Accepted Dec 23, 2022

### Keywords:

Color uniformity

$\text{LaAlO}_3:\text{Dy}^{3+}$

Luminous flux

White LED

X-ray analysis

## ABSTRACT

$\text{LaAlO}_3:\text{Dy}^{3+}$  ( $\text{LAO}:\text{Dy}^{3+}$ ) with blue-yellow emission for brilliant white light of light-emitting diodes (LEDs) was prepared using gel-combustion process. The chemical content of the created material was confirmed using energy dispersive X-ray analysis (EDX). The transmission electron microscopy was used to examine the phosphor crystal size and morphology. The luminescence analysis showed that  $\text{LAO}:\text{Dy}^{3+}$  phosphors exhibited peaks at 482 nm (blue) and 574 nm (yellow), attributed to the transitions  $4\text{F } 9/2 \rightarrow 6\text{H } 15/2$  and  $4\text{F } 9/2 \rightarrow 6\text{H } 13/2$ , respectively. The investigating of correlated color temperature (CCT) and Commission International de L'Eclairage (CIE) described that the phosphor  $\text{LAO}:\text{Dy}^{3+}$  helped to attained good CCT coordination and bright cool-white emission under ultraviolet (UV) stimulation. However, when using in white LED fabrication, the concentration of  $\text{LAO}:\text{Dy}^{3+}$  should be modified to fulfill the need from manufactures. According to results from this work, the white light luminescence intensity and color rendering performance may be reduced if the  $\text{LAO}:\text{Dy}^{3+}$  is high ( $>10\%$ ) because of too much scattering. On the other hand, such scattering improvements offered by  $\text{LAO}:\text{Dy}^{3+}$  phosphor is beneficial to reduce the color deviance for better color uniformity of light.

This is an open access article under the [CC BY-SA](#) license.



## Corresponding Author:

Huu Phuc Dang

Faculty of Fundamental Science, Industrial University of Ho Chi Minh City

No. 12 Nguyen Van Bao Street, Ho Chi Minh City, Vietnam

Email: danghuuphuc@iuh.edu.vn

## 1. INTRODUCTION

Over the last several decades, there has been a lot of interest in researching luminous materials in order to create efficient phosphors with high luminescent output and good thermal and chemical performances [1], [2]. These phosphor materials have a wide range of applications, such as fluorescence lights, solid-state illuminating technology, liquid crystal displays, white light-emitting diodes (WLEDs), and sensors [3]. WLEDs provide several advantages over traditional illumination types, including a shorter operation time, better lifetime, greater brightness, and much lower energy-consumption level [4]. Phosphor materials can emit light, or display luminescence, when excited by particle or electromagnetic radiation. The photoluminescence characteristics of rare-earth-doped compounds are affected by the host material's restricted structure and composition [5]. Besides, current studies in the research aspect have discussed the performance of lanthanide (Ln) luminescence in diverse hosts based on phosphates, borates, aluminates, and silicates [6], [7]. Ln-doped-aluminates stand out among the mentioned compounds because of their simple synthesis, strong luminous efficiency, viable structural characteristics, and spectacular thermal and chemical robustness. The  $\text{ABO}_3$  perovskite-type materials, which have good chemical and physical stability and a diversity of structural and compositional characteristics, can be served as the excellent hosts for WLED

phosphors.  $\text{LaAlO}_3$  (LAO) is one of the potential host materials for conversion phosphors, a substrate for superconductors, a giant magneto-resistive material, and magnetic thin sheets due to its broad bandgap and noticeably low photon power [8], [9]. The white emission of  $\text{LaAlO}_3:\text{Dy}^{3+}$  (LAO: $\text{Dy}^{3+}$ ) nanomaterial draws a lot of attention owing to the strong line of emission of  $\text{Dy}^{3+}$  exhibiting in the visible spectral regions of yellow (574 nm,  $4\text{F}_{9/2} \rightarrow 6\text{H}_{13/2}$ ) and blue (482 nm,  $4\text{F}_{9/2} \rightarrow 6\text{H}_{15/2}$ ) [10], [11]. The combination of these two colors, yellow and blue, produces brilliant white light that is used in a variety of applications such as light-emitting diodes (LEDs), paints, optoelectronic devices, and current displays [12]. Bright white light produced by the combination of these two colors, yellow and blue, can be used in a variety of products, including LEDs, paints, optoelectronic devices, and contemporary displays [13], [14].

In this study, the nanomaterial is suggested and created using low-temperature gel-combustion technique. The characterizing process of single-phase LAO: $\text{Dy}^{3+}$  perovskite phosphor was carried out using various measurement instruments. Specifically, in order to support the use of LAO: $\text{Dy}^{3+}$  WLEDs, the phosphor luminescence characteristics were studied by X-ray diffraction (XRD), transmission electron microscope (TEM), fourier transform infrared (FTIR), energy dispersive X-ray (EDX), and photoluminescent spectroscopy. The data outcome indicates that LAO: $\text{Dy}^{3+}$  phosphors are prospective materials for white LEDs due to their beneficial luminescent properties.

## 2. METHOD

### 2.1. Phosphor synthesizing process

The synthesizing method for LAO: $\text{Dy}^{3+}$  phosphor samples is the gel combustion method. Chemical ingredients for LAO: $\text{Dy}^{3+}$  synthesis are  $\text{La}(\text{NO}_3)_3 \cdot 6\text{H}_2\text{O}$ ,  $\text{H}_{12}\text{DyN}_3\text{O}_{15}$ ,  $\text{Al}(\text{NO}_3)_3 \cdot 9\text{H}_2\text{O}$ , and  $\text{C}_6\text{H}_{12}\text{N}_4$ .  $\text{C}_6\text{H}_{12}\text{N}_4$  or hexamine is used as a reducer in the synthesis process [15], [16]. When these metal nitrates were dissolved in de-ionized water, they released active oxygen acting as an oxidizing agent. The raw ingredients were initially blended to form a uniform solution in a silica crucible. Then, the mixture was heated at around 80 °C to attain an adhesive solution. Subsequently,  $\text{C}_6\text{H}_{12}\text{N}_4$  was added with distilled water into a plate and heated with magnetic stirrer until the solution become a gel.  $\text{C}_6\text{H}_{12}\text{N}_4$  was dissolved uniformly to frame a metal compound in the chemical reaction process. Next, the solution was heated at 600 °C in a furnace for around 12 minutes. Material combustion involves self-sustaining, decomposition, dehydration, and the liberation of gases including nitrogen, ammonia, and  $\text{CO}_2$ . Because of the evolution of gases, the created phosphor sample became scruffy with embrasure in nanoparticles. The nanoparticles' crystallinity is influenced by the self-sustaining exothermal reactive combustion. Additionally, the lower temperature of the synthesizing process affects the size of phosphor granules. The as-prepared phosphor sample was heated again for 2h at temperatures of 800 °C and 1,000 °C for further investigation on the optoelectronic characteristics and crystallinity.

### 2.2. Essential measurement instruments

The list of instruments used in the phosphor-property analysis was detailed in Table 1. The Rigaku XRD is operated with tube voltage of 40 kV and tube current of 30 mA, the Cu wavelength ( $\text{K}\alpha 1$ ) of about 1.54 Å. The Tecnai TEM from field electron and ion company (FEI) company United State of America (USA) uses a 200-kV field-emission gun. The Horiba spectrofluorometer use a xenon lamp as its excitation source [17].

Table 1. Instrument used for investigating phosphor LAO: $\text{Dy}^{3+}$

Instruments	Model	Investigation on
XRD	Rigaku Ultima-IV	Phase purity and lattice structure
FTIR spectroscopy	Nicolet iS50	Crystal bonding in the lattice
TEM	FEI Tecnai	Morphology and particle size
EDX spectrometer	Ametek EDX	Elemental investigation
Spectrofluorometers	Horiba Fluorolog (Jobin YVON)	Luminescence

### 2.3. WLED simulation

LAO: $\text{Dy}^{3+}$  phosphor was applied to build the model of two-remote-phosphor-layer WLED, in addition to the YAG: $\text{Ce}^{3+}$  phosphor, which is depicted in Figure 1. The actual WLED model was displayed in Figure 1(a). The phosphor-layer cluster was placed over the blue-chip set, as shown in Figure 1(b). Figures 1(c) and 1(d) illustrated the diagram of chip wire-bonding and the WLED's 3D model by LightTools software [18]–[20], respectively.

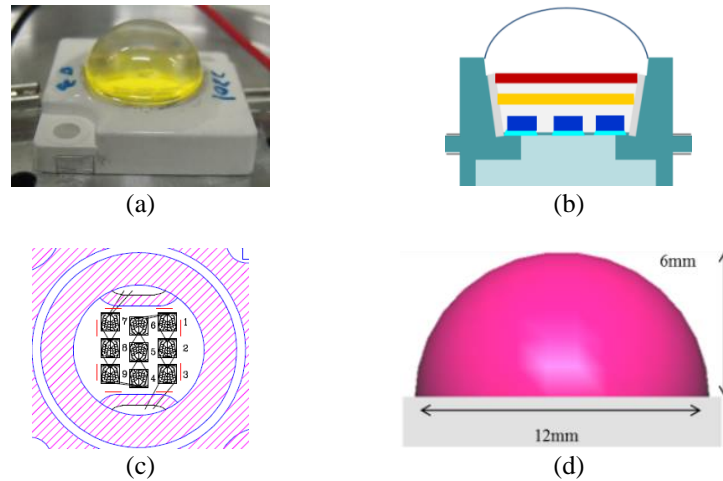


Figure 1. Photograph of WLEDs structure: (a) actual WLEDs, (b) bonding diagram, (c) illustration of pc-WLEDs model, and (d) simulation of WLEDs using LightTools commercial software

### 3. RESULTS AND DISCUSSION

#### 3.1. Computation

Through X-ray analysis, it showed no-peak the XRD pattern, indicating the remained bulk structure of the LAO lattice when integrating the ion dopant  $\text{Dy}^{3+}$ . The event that ion  $\text{Dy}^{3+}$  replaced the  $\text{La}^{3+}$  site of the host could be attributed to their same charge by their ionic-radius percentage difference ( $D_{ir}$ ), as expressed [21],

$$D_{ir} = \frac{R_{la}(INC) - R_{do}(INC)}{R_{la}(INC)} \times 100\% \quad (1)$$

where the ionic radii of the dopant ( $R_{do}$ )  $\text{Dy}^{3+}$  ion is 1.16 Å and of the lattice ion  $\text{La}^{3+}$  ( $R_{la}$ ) is 1.027 Å. Additionally,  $INC$  represents the number of coordination of a specific ion. The  $D_r$  here is computed to be about 11.47%, while the acceptable  $D_r$  can be up to 30%, indicating that the appropriate replacement of  $\text{Dy}^{3+}$  with  $\text{La}^{3+}$  in the LAO lattice.

The particle size of the phosphor ( $D_{hkl}$ ) from the full width-half maximum (FWHM) of the most intense peak ( $\beta$ ) in the pattern of XDR can be determined with the Debye-Scherrer expression in (2) [22],

$$D_{hkl} = \frac{(k\lambda)}{[\beta(2\theta)\cos\theta]} \quad (2)$$

where  $k$  is constant and equal to 0.89,  $\lambda$  is the  $\text{CuK}\alpha$  wavelength and equal to 0.154 nm, and  $\theta$  is the angle of diffraction. The calculated particle size of the phosphor was recorded to be around 19–30 nm. The crystallinity and particle size of the phosphor increased with the increasing annealed temperature, referring to the higher intensity of the peak in the X-ray pattern. Both particle size and strain contribute to this spectral line broadening. Using Williamson-Hall equation, the phosphor lattice micro-strain can be computed, as expressed in (3) and rearranged in (4) [23].

$$\beta_{hkl} = \frac{(K\lambda)}{(D \cos \theta)} + 4\varepsilon \tan \theta \quad (3)$$

$$\beta_{hkl} \times \cos \theta_{hkl} = \frac{K\lambda}{D} + 4\varepsilon \sin \theta_{hkl} \quad (4)$$

where  $\beta_{hkl}$  represents the FWHM of the strong peak,  $K$  and  $D$  are constants, and  $\varepsilon$  is the arising line broadening caused by the strain in the lattice.

The critical distance ( $R_{ct}$ ) of energy transferring among the ions in the lattice is used to analyze the quenching mechanism of dopant concentration. The Blasse relation is applied to calculate  $R_{ct}$ , as expressed in (5) [24],

$$R_{ct} = 2 \times \left( \frac{3V}{4\pi X_{ct}Z} \right)^{1/3} \quad (5)$$

where  $Z$  and  $V$  are the unit-cell number of  $\text{Dy}^{3+}$  replaceable sites and volume, which are equal to 4 and 54.39 Å<sup>3</sup>, respectively, and  $X_{ct}$  is  $\text{Dy}^{3+}$  critical concentration and equal to 0.04. As a result, the calculated  $R_{ct}$  is

larger than 5 Å. Meanwhile, the exchange interaction is accountable for the energy transferring mechanism of the ion when the  $R_{ct}$  is within 3-4 Å. With  $R_c$  larger than this range, the energy transfer is caused by the multipolar interactions. The relation between luminescent strength ( $S$ ) and the concentration of  $Dy^{3+}$  ion ( $x$ ) can be described using the following (6) and re-arranged for computation in (7) [25],

$$S/x = k \times (1 + \beta x^{t/3})^{-1} \quad (k \text{ and } \beta \text{ are constant values}) \quad (6)$$

$$\log(S/x) = k - (t/3) \log(x) \quad (7)$$

from which the kind of multipolar interaction for energy transfer among ions in the lattice was determined to be the dipole-dipole as the  $t$ -value was computed to be around 6.27.

### 3.2. Effects on white LED illumination features

When  $LAO:Dy^{3+}$  is used as an additional phosphor film in the package, the scattering activity of emission light is affected. Figure 2 shows the reduced scattering coefficients regarding the increase in  $LAO:Dy^{3+}$  concentration (10-50%). The reduced scattering increase with the concentration of the added phosphor, meaning that scattering efficient is not supported at high phosphor concentration, especially in the case of emitted light with lower wavelength (blue light emission). As a result, the luminous intensity and correlated color temperature (CCT) values of the WLED changes.

Figure 3 presents the change of YAG:Ce phosphor concentration when the  $LAO:Dy^{3+}$  phosphor increase in its concentration. The inverse movement between their concentration is clearly show. YAG:Ce decreases its content along the increasing  $LAO:Dy^{3+}$  concentration to stabilize the CCT value at a desired level. Subsequently, the CCT values changing with  $LAO:Dy^{3+}$  concentrations were analyzed and depicted in Figure 4. As the content of  $LAO:Dy^{3+}$  becomes larger, the CCT tends to be more stable and present smaller difference between the highest and lowest CCT points. This difference is referred as to the CCT deviation (D-CCT), as depicted in Figure 5. The data from Figure 5 obviously show the notable drop in D-CCT when the concentration of  $LAO:Dy^{3+}$  increase from 0% to 10%. After that, the significant fluctuation is observed but the results are still much lower than when there is no  $LAO:Dy^{3+}$  in the packages. The D-CCT bottoms out at  $LAO:Dy^{3+}$  concentration equal to 30%. This result implies that  $LAO:Dy^{3+}$  is a good material to keep good CCT coordination.

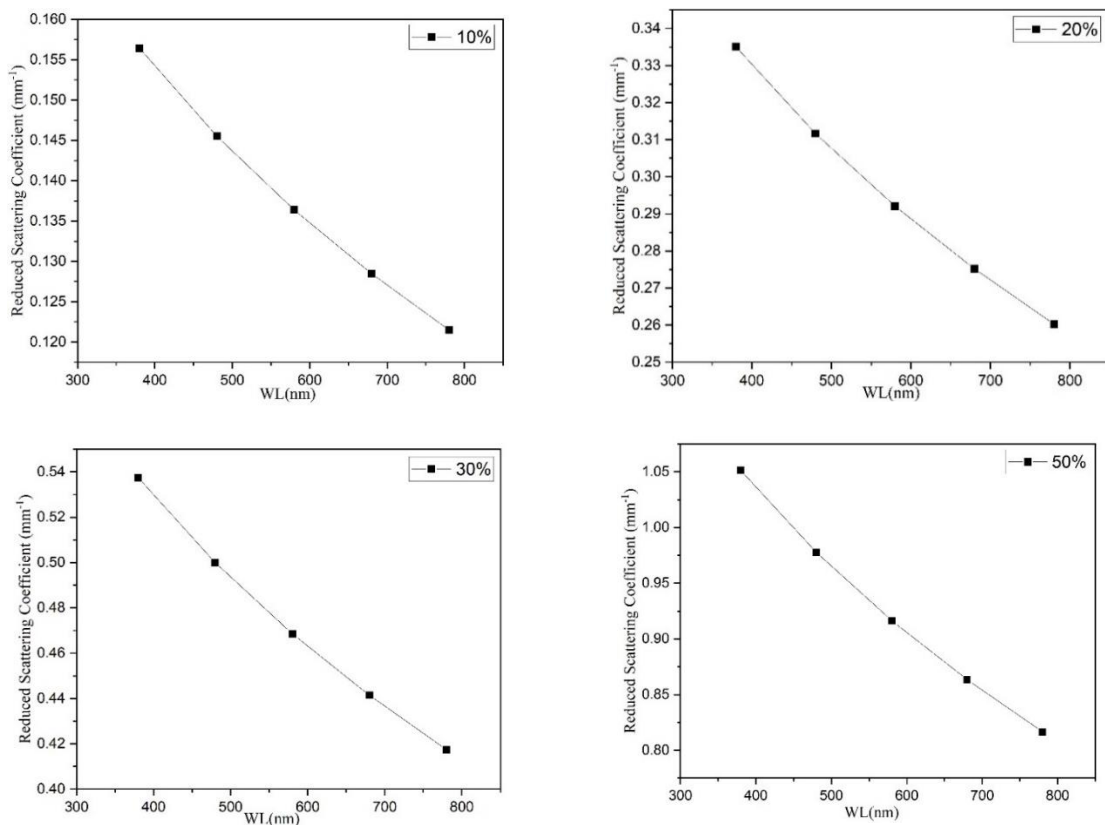


Figure 2. Reduced scattering coefficient with changes in  $LAO:Dy^{3+}$  concentration

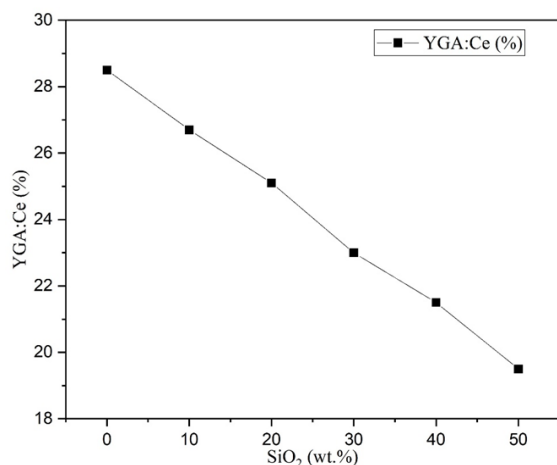


Figure 3. YAG:Ce content with increasing LAO:Dy<sup>3+</sup> concentration

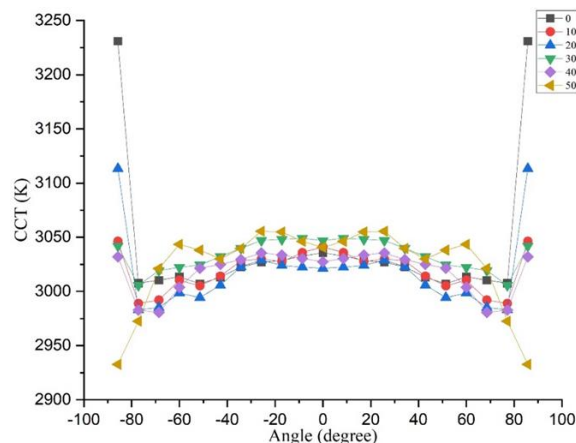


Figure 4. CCT of the white light with increasing LAO:Dy<sup>3+</sup> concentration

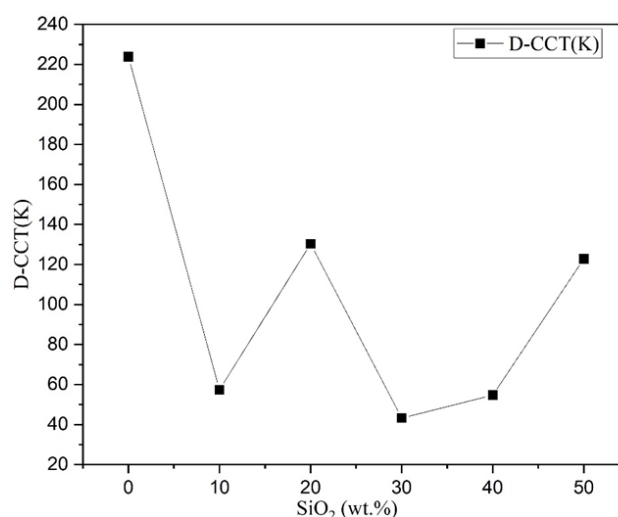


Figure 5. D-CCT of the white light with increasing LAO:Dy<sup>3+</sup> concentration

Figure 6 shows the emission spectra of white light when the phosphor LAO:Dy<sup>3+</sup> is added. The emission peaks are observed in the blue (482 nm) and yellow (574 nm) wavelength areas. However, the emission power shows reduction at higher LAO:Dy<sup>3+</sup> concentration. Figure 7 further demonstrates the lumen output of the white emission of the LED as a function of varying LAO:Dy<sup>3+</sup> (10-50%). The increasing concentration of the phosphor show no favor to the luminous efficacy as the line graph is generally show downward tendency when the concentration of LAO:Dy<sup>3+</sup> starts to increase. This maybe attributed to the reduced scattering efficiency as there is no sufficient forward scattering of blue emission when the concentration of LAO:Dy<sup>3+</sup> increase. The backward scattering seems to arise and develop, leading to reflection and self-absorption of the phosphor material [26]. Thus, the total emission power is degraded.

Next, the color rendition performance of the white LED with increasing concentration of LAO:Dy<sup>3+</sup> are discussed with two parameters: color rendering index (CRI) in Figure 8 and color quality scale (CQS) in Figure 9. Both figures depict the decline as we increase the utilized content of LAO:Dy<sup>3+</sup> phosphor. This phenomenon is understandable because in the emission spectral band of white light when using LAO:Dy<sup>3+</sup> phosphor (see Figure 6), the red spectra is not covered sufficiently to support the color reproduction. Nevertheless, the phosphor gives good CCT coordination and lumen when using at around 10% concentration. Thus, we can use the phosphor to fabricate bright-white light for LED applications.

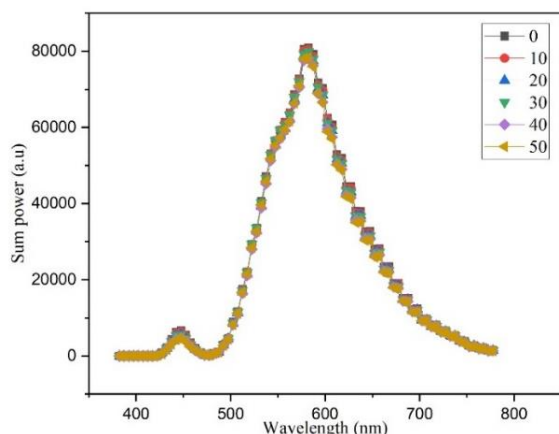


Figure 6. Emission spectra of the white light with increasing LAO:Dy<sup>3+</sup> concentration

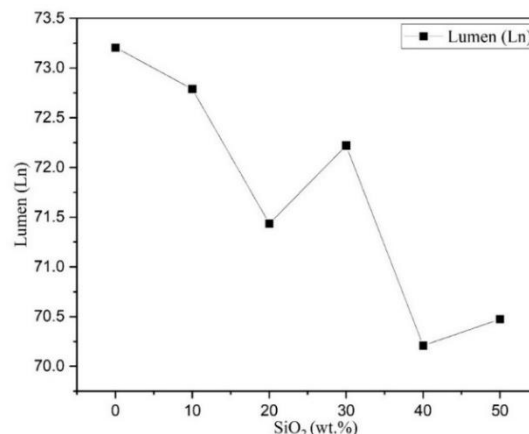


Figure 7. The lumen intensity of the white light with increasing LAO:Dy<sup>3+</sup> concentration

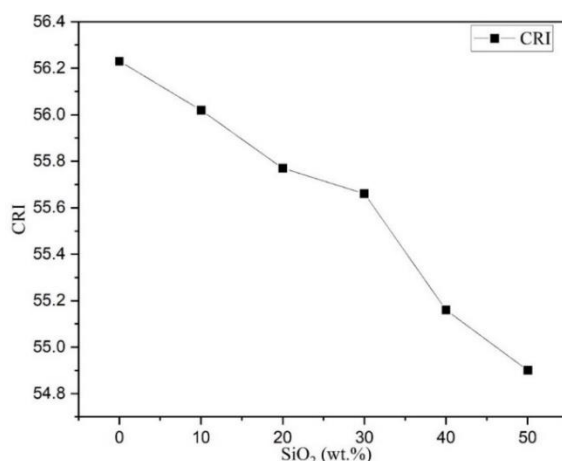


Figure 8. CRI of the white light with increasing LAO:Dy<sup>3+</sup> concentration

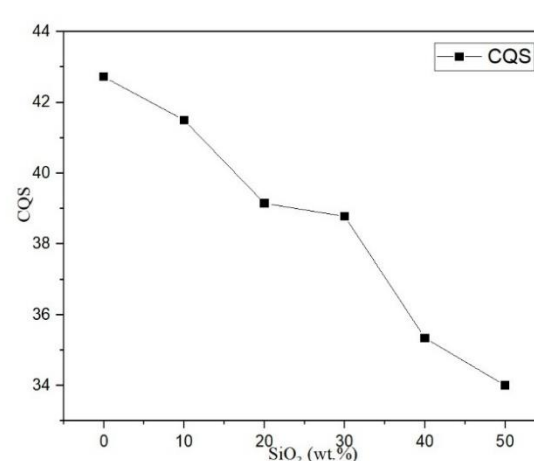


Figure 9. CQS of the white light with increasing LAO:Dy<sup>3+</sup> concentration

#### 4. CONCLUSION

The LaAlO<sub>3</sub>:Dy<sup>3+</sup> nanoparticles were created using the gel-combustion method. The TEM image revealed the development of nanocrystals in the range of 11–30 nm. The absence of peaks in EDX spectral intensity corresponds to external components, which contributes to confirming the material pure synthesis. Under an excitation wavelength of 351 nm, it recorded two prominent peaks in blue (482 nm) and yellow (574 nm) areas, which were assigned to 4F 9/2→6H 15/2 and 4F 9/2→6H 13/2, respectively. The critical distance was determined using Blasse relation, showing the effective energy transmission via the dipole-dipole multipolar interaction mechanism. The Commission International de L'Eclairage (CIE) coordinates and CCT levels were recorded in the vivid white zone, indicating the potential and suitability of LAO:Dy phosphors for WLEDs.

#### REFERENCES




- [1] T. Kozacki, M. Chlipala, and P. L. Makowski, "Color Fourier orthoscopic holography with laser capture and an LED display," *Optics Express*, vol. 26, no. 9, pp. 12144–12158, Apr. 2018, doi: 10.1364/OE.26.012144.
- [2] J. Li, F. Wang, M. Zhao, F. Jiang, and N. Chi, "Large-coverage underwater visible light communication system based on blue LED employing equal gain combining with integrated PIN array reception," *Applied Optics*, vol. 58, no. 2, pp. 383–388, Jan. 2019, doi: 10.1364/AO.58.000383.
- [3] A. Lihachev, E. V. Plorina, M. Lange, I. Lihacova, A. Derjabo, and D. Bliznuks, "Imaging of LED-excited autofluorescence photobleaching rates for skin diagnostics," in *Clinical and Preclinical Optical Diagnostics II*, Jul. 2019, p. 63, doi: 10.1117/12.2526260.
- [4] H. Liu *et al.*, "TuLUMIS-a tunable LED-based underwater multispectral imaging system," *Optics Express*, vol. 26, no. 6, pp. 7811–7828, Mar. 2018, doi: 10.1364/OE.26.007811.
- [5] R. H. Horng, S. Sinha, C. P. Lee, H. A. Feng, C. Y. Chung, and C. W. Tu, "Composite metal substrate for thin film AlGaInP LED applications," *Optics Express*, vol. 27, no. 8, pp. 397–403, Apr. 2019, doi: 10.1364/OE.27.00A397.
- [6] P. Manley, S. Walde, S. Hagedorn, M. Hammerschmidt, S. Burger, and C. Becker, "Nanopatterned sapphire substrates in deep-






- UV LEDs: is there an optical benefit?," *Optics Express*, vol. 28, no. 3, pp. 3619–3635, Feb. 2020, doi: 10.1364/OE.379438.
- [7] X.-X. Xia *et al.*, "LED-based fiber quantum key distribution: toward low-cost applications," *Photonics Research*, vol. 7, no. 10, pp. 1169–1174, Oct. 2019, doi: 10.1364/PRJ.7.001169.
  - [8] Q. H. Pham, J. C. Chen, and H. B. Nguyen, "Reducing efficiency droop in (In,Ga)N/GaN light-emitting diodes by improving current spreading with electron-blocking layers of the same size as the N-pad," *Current Optics and Photonics*, vol. 4, no. 4, pp. 380–390, 2020, doi: 10.3807/COPP.2020.4.4.380.
  - [9] J. Yan *et al.*, "Uniting GaN electronics and photonics on a single chip," *Journal of Lightwave Technology*, vol. 39, no. 19, pp. 6269–6275, Oct. 2021, doi: 10.1109/JLT.2021.3094850.
  - [10] C. Zhao, C. W. Tang, B. Lai, G. Cheng, J. Wang, and K. M. Lau, "Low-efficiency-droop InGa<sub>N</sub> quantum dot light-emitting diodes operating in the 'green gap,'" *Photonics Research*, vol. 8, no. 5, pp. 750–754, May 2020, doi: 10.1364/PRJ.380158.
  - [11] B. Tang, L. Gong, H. Hu, H. Sun, and S. Zhou, "Toward efficient long-wavelength III-nitride emitters using a hybrid nucleation layer," *Optics Express*, vol. 29, no. 17, pp. 27404–27415, Aug. 2021, doi: 10.1364/OE.430721.
  - [12] C. Liu, Y. Cai, H. Jiang, and K. M. Lau, "Monolithic integration of III-nitride voltage-controlled light emitters with dual-wavelength photodiodes by selective-area epitaxy," *Optics Letters*, vol. 43, no. 14, pp. 3401–3404, Jul. 2018, doi: 10.1364/OL.43.003401.
  - [13] M. S. Wong *et al.*, "High efficiency of III-nitride micro-light-emitting diodes by sidewall passivation using atomic layer deposition," *Optics Express*, vol. 26, no. 16, pp. 21324–21331, Aug. 2018, doi: 10.1364/OE.26.021324.
  - [14] Y. Park, K. H. Li, W. Y. Fu, Y. F. Cheung, and H. W. Choi, "Packaging of InGa<sub>N</sub> stripe-shaped light-emitting diodes," *Applied Optics*, vol. 57, no. 10, pp. 2452–2458, Apr. 2018, doi: 10.1364/AO.57.002452.
  - [15] K. Gibasiewicz *et al.*, "InGa<sub>N</sub> blue light emitting micro-diodes with current path defined by tunnel junction," *Optics Letters*, vol. 45, no. 15, pp. 4332–4335, Aug. 2020, doi: 10.1364/OL.394629.
  - [16] X. Tao *et al.*, "Performance enhancement of yellow InGa<sub>N</sub>-based multiple-quantum-well light-emitting diodes grown on Si substrates by optimizing the InGa<sub>N</sub>/Ga<sub>N</sub> superlattice interlayer," *Optical Materials Express*, vol. 8, no. 5, pp. 1221–1230, 2018, doi: 10.1364/OME.8.001221.
  - [17] K. H. Li *et al.*, "Monolithically integrated InGa<sub>N</sub>/Ga<sub>N</sub> light-emitting diodes, photodetectors, and waveguides on Si substrate," *Optica*, vol. 5, no. 5, pp. 564–569, May 2018, doi: 10.1364/OPTICA.5.000564.
  - [18] C. F. Fong *et al.*, "Silicon nitride nanobeam enhanced emission from all-inorganic perovskite nanocrystals," *Optics Express*, vol. 27, no. 13, pp. 18673–18682, Jun. 2019, doi: 10.1364/OE.27.018673.
  - [19] V. Ryzhii *et al.*, "Theoretical analysis of injection driven thermal light emitters based on graphene encapsulated by hexagonal boron nitride," *Optical Materials Express*, vol. 11, no. 2, pp. 468–486, Feb. 2021, doi: 10.1364/OME.412973.
  - [20] P. S. Yeh, Y.-C. Chiu, T.-C. Wu, Y.-X. Chen, T.-H. Wang, and T.-C. Chou, "Monolithic integration of Ga<sub>N</sub>-based phototransistors and light-emitting diodes," *Optics Express*, vol. 27, no. 21, pp. 29854–29862, Oct. 2019, doi: 10.1364/OE.27.029854.
  - [21] B. Jain, R. T. Velpula, M. Patel, and H. P. T. Nguyen, "Controlled carrier mean free path for the enhanced efficiency of III-nitride deep-ultraviolet light-emitting diodes," *Applied Optics*, vol. 60, no. 11, pp. 3088–3093, Apr. 2021, doi: 10.1364/AO.418603.
  - [22] N. K. Manjunath, Y. Lu, and S. Lin, "Van der Waals contacted MoO<sub>x</sub> stacked ZnO/GaN vertical heterostructured ultraviolet light emitting diodes," *Optics Express*, vol. 28, no. 21, pp. 31603–31610, Oct. 2020, doi: 10.1364/OE.402261.
  - [23] D. Durmus and W. Davis, "Blur perception and visual clarity in light projection systems," *Optics Express*, vol. 27, no. 4, pp. 216–223, Feb. 2019, doi: 10.1364/OE.27.00A216.
  - [24] W. Bao, M. Wei, and K. Xiao, "Investigating unique hues at different chroma levels with a smaller hue angle step," *Journal of the Optical Society of America A*, vol. 37, no. 4, pp. 671–679, Apr. 2020, doi: 10.1364/JOSAA.383002.
  - [25] H. Jiang *et al.*, "Projection optical engine design based on tri-color LEDs and digital light processing technology," *Applied Optics*, vol. 60, no. 23, pp. 6971–6977, Aug. 2021, doi: 10.1364/AO.432355.
  - [26] Z. Zhao, H. Zhang, S. Liu, and X. Wang, "Effective freeform TIR lens designed for LEDs with high angular color uniformity," *Applied Optics*, vol. 57, no. 15, pp. 4216–4221, May 2018, doi: 10.1364/AO.57.004216.

## BIOGRAPHIES OF AUTHORS



**Ha Thanh Tung**    received the PhD degree in physics from University of Science, Vietnam National University Ho Chi Minh City, Vietnam, he is working as a lecturer at the Faculty of Basic Sciences, Vinh Long University of Technology Education, Vietnam. His research interests focus on developing the patterned substrate with micro- and nano-scale to apply for physical and chemical devices such as solar cells, OLED, photoanode. He can be contacted at email: tunght@vlute.edu.vn.



**Huu Phuc Dang**    received a Physics Ph.D degree from the University of Science, Ho Chi Minh City, in 2018. Currently, he is a lecturer at the Faculty of Fundamental Science, Industrial University of Ho Chi Minh City, Ho Chi Minh City, Vietnam. His research interests include simulation LEDs material, renewable energy. He can be contacted at email: danghuuphuc@iuh.edu.vn.